Integrating Compositional and Structural Diversity in Heterometallic Titanium Frameworks by Metal Exchange Methods.

Eloy P. Gómez-Oliveira,[a] Javier Castells-Gil,[b] Clara Chinchilla-Garzón,[a] Andrés Uscategui-Linares,[c] Josep Albero,[c] Neyvis Almora-Barrios,[a] Sergio Tatay,[a] Natalia M. Padial,[a]* and Carlos Martí-Gastaldo.[a]*

[a] Universidad de Valencia (ICMol). Catedrático José Beltrán-2, 46980, Paterna (Spain)

[b] School of Chemistry, University of Birmingham. Edgbaston, Birmingham, B152TT, (United Kingdom)

[c] Instituto Universitario de Tecnología Química CSIC-UPV, Universitat Politècnica de València. Av. De los Naranjos s/n, 46022, Valencia (Spain).

KEYWORDS: Titanium Frameworks, Metal Exchange, Post-Synthetic Modification, Heterometallic Cluster, Mesoporosity

ABSTRACT: The increasing use of Metal-Organic Frameworks (MOFs) in separation, catalysis or storage is linked to the targeted modification of their composition or porosity metrics. While modification of pore shape and size necessarily implies the assembly of alternative nets, compositional changes often rely on post-synthetic modification adapted to the functionalisation or exchange of the organic linker, or the modification of the inorganic cluster by metal exchange methods. We describe an alternative methodology that enables the integration of both types of modification, structural and compositional, in titanium MOFs by metal exchange reaction of the heterometallic cluster Ti_2Ca_2. A systematic analysis of this reactivity with MUV-10 is used to understand which experimental variables are crucial to enable replacement of calcium only, or to integrate metal exchange with structural transformation. The isoreticular expanded framework MUV-30, is next used to template the formation of MUV-301, a titanium framework not accessible by direct synthesis that displays the largest mesoporous cages reported to date. Given that the interest of Ti MOFs in photoredox applications often meets the limitations imposed by the challenges of titanium solution chemistry to design concrete candidates, this soft strategy based on pre-assembled frameworks will help integrating specific combinations of metals into high porosity architectures.

INTRODUCTION

The design and synthesis of reticular frameworks continues to grow.[1] Beyond their interest in separation,[2–4] adsorption[5–7] and catalysis[8,9] technologies, mostly based on their high intrinsic porosity, the diversification in the structure and composition of this family of porous materials is based on two fundamental characteristics. First, the assembly of this type of architecture follows almost arithmetic principles, in which the construction of different topologies is dictated by the structural information encoded by the symmetry and connection points of the molecular blocks that act as organic and inorganic nodes, respectively.[10,11] In addition, this design strategy can be made compatible with a wide variety of organic functional groups and discrete metals or combinations thereof, for a broad range of porous, crystalline solids with compositional diversity unmatched by any other family of synthetic materials. Beyond chemical complexity, this compositional diversity also has a direct impact on the properties of Metal-Organic and Covalent-Organic Frameworks (MOFs and COFs), allowing the modification of their catalytic,[12–15] optical,[16,17] electrical,[18,19] chiral,[20,21] mechanical robustness,[22,23] chemical stability,[24,25] structural flexibility,[26,27] and ability to separate, store, and release specific molecules.

This compositional diversification to gain control over MOF function has gone hand in hand with the development of post-synthetic methodologies[28] that enable the integration of multiple components that are often inaccessible by direct synthesis (**Figure 1, left**). Methodologically, these strategies are designed according to the nature of the building blocks to be modified. For example, the pioneering work of Cohen and co-workers has contributed to the expansion of the functional groups scope of the scaffold by post-synthetic covalent modification of reactive tags in the organic linker.[29] This method was rapidly adopted as a general route for functionalizing frameworks, provided that appropriate reagents and reaction conditions are chosen to allow modification of the pore chemistry without altering the structure or porosity of the material.[30] Beyond the modification of molecular building blocks, other routes, such as solvent-assisted linker exchange (SALE),[31–33] allow the incorporation of one or more organic linkers by replacing pre-existing ones, exploiting the lability of coordination linkages under conditions suitable for the controlled exchange of units and their diversification. From an inorganic point of view, compositional tunability has focused mainly on metal exchange or transmetalation reactions to partially or completely replace some or all the metal positions in the metal clusters in the framework.[34,35]

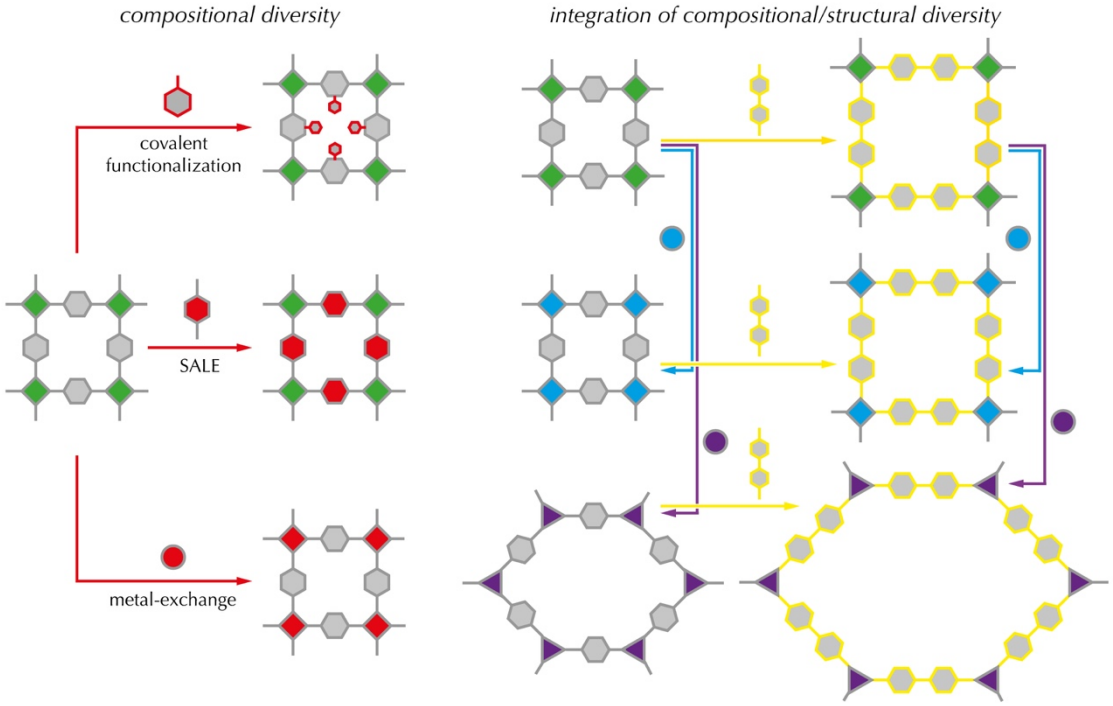

Figure 1. *Left*: Post-synthetic modification routes to modify MOF chemical composition without altering their original structure. From top to bottom: covalent functionalization, solvent-assisted linker exchange, and metal exchange reactions. The modification of the original composition is highlighted in red. *Right*: Integration of compositional and structural diversity by metal exchange methods. The yellow line connects isoreticular augmented frameworks. Both are compatible with the formation of mixed metal clusters by metal exchange (blue line stands for compositional diversification) and the formation of alternative topologies dictated by the formation of a new cluster with different nuclearity and connection points (purple line, compositional and structural diversification).

All these strategies are generally used to diversify the chemical composition and control of MOF function with a common characteristic, they do so without altering the structure and porosity of the resulting material which is fixed by the topology of the starting framework. However, what if both aspects could be integrated in the same post-synthetic modification to integrate the structural and compositional changes for a given framework? As a continuation of our previous results,[36] in this work, we generalize the use of metal-exchange reactions for heterometallic clusters not restricted exclusively to varying compositions but also useful to directing the formation of ultraporous titanium frameworks inaccessible by direct methods (**Figure 1, right**).

RESULTS AND DISCUSSION

Systematic approach to metal exchange reactions with Ti_2Ca_2 clusters.

Our previous work with MUV-10 showed how the combination of hard (Ti^{4+}) and soft (Ca^{2+}) metal centers in the heterobimetallic cluster $[Ti_2Ca_2(O)_2(H_2O)_4(RCO_2)_8] \equiv (Ti_2Ca_2)$ led to an atypical behavior when reacted with late divalent metals of the first transition series (Mn, Fe, Co, Ni, Cu, and Zn).[36] Compared to other soft metal-based frameworks based on Zn(II) clusters such as MOF-5,[35] MFU-4l,[37] ZIF-8,[38] PMOF-2[39] or PCN-921,[40] (**Figure 2a**) in which the reaction of the starting crystals allows partial or quantitative replacement of the starting metals without altering the original structure, the reaction of MUV-10 crystals[41] under similar conditions leads to the formation of new materials as a result of quantitative calcium exchange for concomitant transformation of the original cluster into heterobimetallic trimers or dimers for the formation of alternative **mtn** MUV-101 (**Figure 2b**) or **tbo** MUV-102 nets. We coined this phenomenology as dynamic topological transformation because of the possibility of controlling it with reaction time; however, we did not delve into controlling the phenomenon from an experimental point of view. Because the metal exchange reaction requires a change in the local coordination sphere, this might be influenced by kinetic and/or thermodynamic factors that could be finely tuned by multiple experimental variables. To try to rationalize this problem, we designed systematic experiments involving variables as particle size (PS), reaction time, concentration (conc.), or temperature (T), as well as the effect of the counter ion and solvent, all considered relevant according to previous work in this context.[42] For clarity, we restricted the experiments to Co^{2+} exchange reactions, which according to our previous results proceed more slowly compared to other metals and would be easier to follow. As shown in **Figure 2c**, three batches of micrometric crystals were prepared under different conditions to investigate the effect of particle size (PS). Two titanium precursors with different stabilities towards hydrolysis, isopropoxide or cyclopentadienyl chloride, were combined with varying concentrations of acetic acid, to produce batches of micrometric crystals by conventional solvothermal synthesis with average sizes of 25 ± 1 (PS1) and 16 ± 9 μm (PS2).[41] In turn, PS3 was prepared by a continuous reagent injection methodology recently described by us,[43] which ensures smaller crystals with an average size of 5 ± 2 μm (**Figure 2d**).

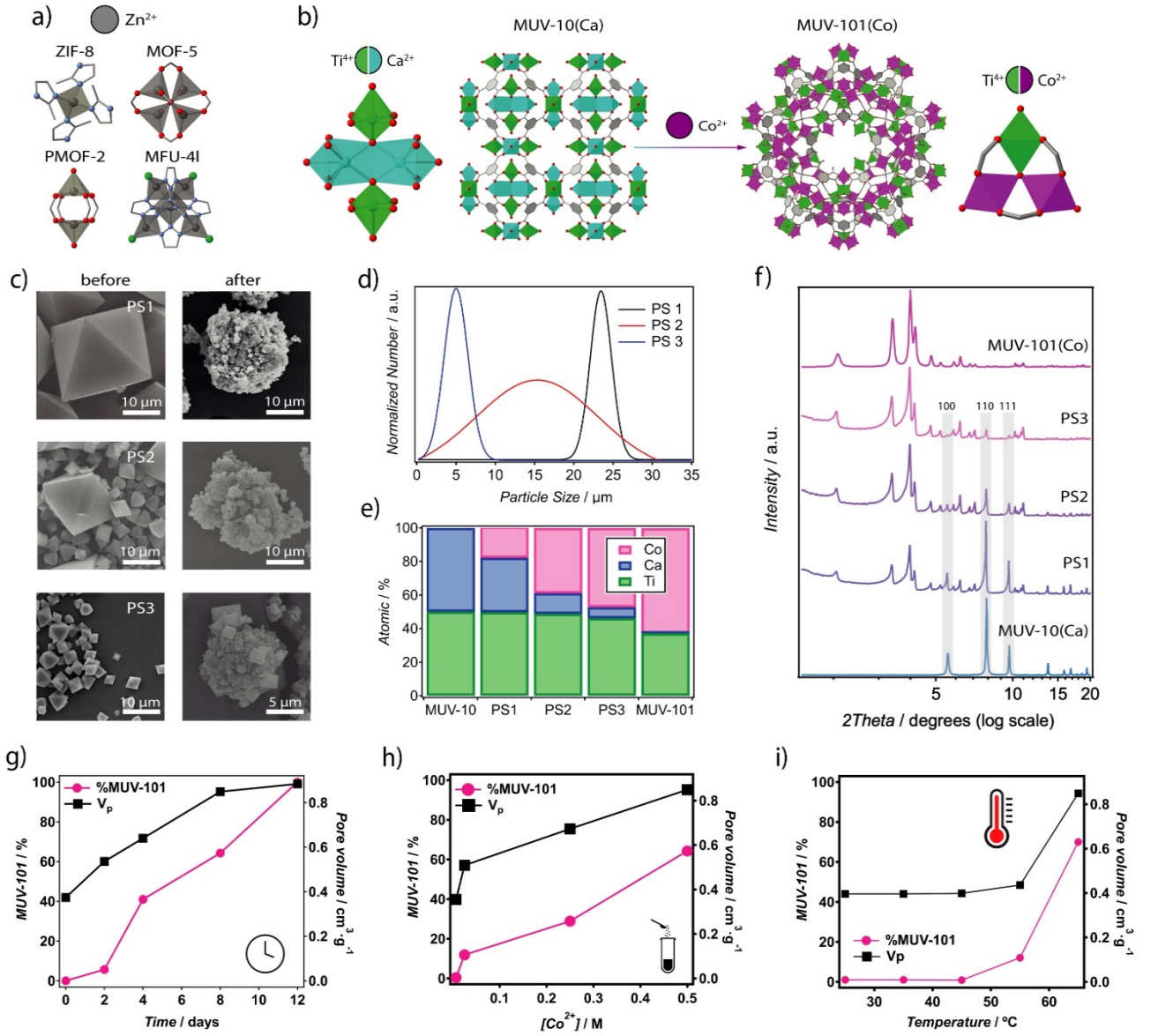

Figure 2. a) Zn(II) homometallic clusters with labile coordination bonds compatible with metal incorporation without structural changes. b) Ti_2Ca_2 heterometallic cluster for which metal exchange reactions induce the formation of a new $TiCo_2$ cluster with consequent structural changes in the framework. c) SEM images of MUV-10 crystals obtained using three different methods before and after the transformation. d) Histogram showing the average size changes for samples PS1, 2 and 3 which show different metal exchange kinetics and structural transformation according to e) ICP-MS and f) X-ray powder diffraction analysis of the isolated materials after 8 days of reaction. The grey strips highlight characteristic hkl reflections of MUV-10. The effects of g) time; (0.2 M Co^{2+}; 65 ºC), h) metal concentration; (8 d; 65 ºC), and i) temperature; (0.2 M Co^{2+}; 8 d) on the transformation of MUV-10(Ca) to MUV-101(Co) were studied in PS1. The analysis was performed based on the phase transformation quantified by Rietveld refinement of the corresponding PXRD patterns and the variation in the experimental pore volume estimated from N_2 adsorption isotherms at 77 K of all the samples analyzed.

100 mg samples of all batches were immersed in a methanolic solution of $Co(NO_3)_2$ 0.2 M and reacted at 65 °C for 8 d in an incubated orbital shaker, followed by centrifugation and thorough washing for their analysis with powder X-ray diffraction (PXRD), scanning electron microscopy (SEM) EDX mapping, ICP-MS, and N_2 gas sorption (**Supplementary Section S3**). **Figure 2e** summarizes the relative variations in Ca, Co, and Ti% obtained by ICP-MS analysis of the isolated solids compared to their nominal values in the MUV-10 and 101 phases. The results suggest an effect of the particle size on the rate of the MUV-10(Ca) → MUV-101(Co) transformation for a faster replacement of Ca with Co as the particle size decreases. This exchange trend agrees with the PXRD patterns, that support the formation of MUV-101 in all cases (**Figure 2f**). The presence of the original MUV-10 phase is much clearer for PS1 crystals of approximately 25 µm compared to PS3 and PS2 for which the transformation is almost complete, suggesting a direct effect of PS in the percentage of MUV-101 formed upon transformation. Based on these results, we opted to use PS3 batches for the experiments described hereafter as it would ensure a faster transformation rate. We studied varying times (0-15 days), concentrations (7 mM-0.5 M), and temperatures (25-65 ºC) of up to 14 different reactions by analyzing the relative percentage of

MUV-10 and 101 phases by Rietveld refinement of the PXRD patterns of all samples and their experimental N_2 pore volumes (**Supplementary Section S5**). Note that a complete transformation into MUV-101 would correspond to 100% of MUV-101 and a V_p of 0.89 $cm^3 \cdot g^{-1}$. **Figures 2g, h, and i** suggest that the three factors have an influence on the kinetics of the reaction, although the transformation profiles show that it requires at least 4 days and temperatures not lower than 65 °C. The concentration range studied also showed a clear influence on the formation of MUV-101 that is favoured at higher concentrations. Although the transformation of the framework is controlled by the formation of a thermodynamically more stable cluster according to our previous results,[36] all these data together suggest that the metal exchange reaction is kinetically controlled. To confirm this point, we also analyzed the effects of the counter ions and solvents. We presumed that they would be important not only in determining the effective concentration of Co^{2+} in solution, but also in facilitating the breaking and forming of coordination bonds necessary to enable the transformation of the Ti_2Ca_2 cluster. We chose three metal salts from monoanionic ligands with varying field strengths according to the spectrochemical series: $Cl^- < NO_3^- < AcO^-$. The experiments were run in parallel at 65 ºC with 0.5 M solutions according to the established protocol. Analysis of the resulting frameworks confirmed that only the nitrate salt led to almost complete transformation compared to acetate for a partial change near to 60%, and chloride was quite ineffective (**Supplementary Section 5.5**). These results suggest that the transformation is not necessarily controlled by trends fixed by the spectrochemical series and other parameters, as the solubility of the salt might also have an influence. As for the role played by the solvent, we conducted the same experiment using 0.5 M solutions of $Co(NO_3)_2 \cdot 6H_2O$ in acetone, 2-propanol, ethanol, and methanol. The results reveal the effect of solvent polarity or relative permittivity on favoring the metal exchange reaction after eight days. Compared with MeOH (ε_r=32.7), for which the transformation was completed, EtOH (24.6) only permitted the formation of a minor fraction of MUV-101, whereas 2-PrOH (19.9) and acetone (0.7) resulted in no significant change (**Supplementary Section 5.6**). These relative differences are consistent with the rates for substitution observed for other carboxylate MOFs,[44] and might suggest an auxiliary effect of MeOH, not only to solvate cations to facilitate their diffusion within the pores of the crystal, but also its ability to act as a coordinating ligand stabilizing the intermediates involved in the break and formation of bonds necessary to drive the transformation of Ti_2Ca_2 into $TiCo_2$ clusters.

We argue that this solvent effect may be used to constrain metal the transformation of the cluster in faviour of a simple replacement of Ca^{2+} ions in the MUV-10 framework. This solvent control would be ideal for diversifying Ti_2M_2 compositions for a given framework and approaching this bimetallic Secondary Building Unit (SBU) to the conventional behavior of other homometallic alternatives (**Figure 3a**). We revisited some of the experimental conditions described above but restricted now to the use of acetone to prevent cluster transformation. Incubation of MUV-10(Ca) with higher concentrations of cobalt (II) nitrate at 55 °C for 15 days resulted in the exchange of nearly 72 % of the calcium ions based on ICP-MS analysis. The PXRD and N_2 isotherms of isolated MUV-10(Co) confirmed a negligible effect on the structure and porosity of the crystals (**Figure 3b** and **3c**). We also performed Focused Ion Beam (FIB) SEM analysis to examine the homogeneity of the exchange at a

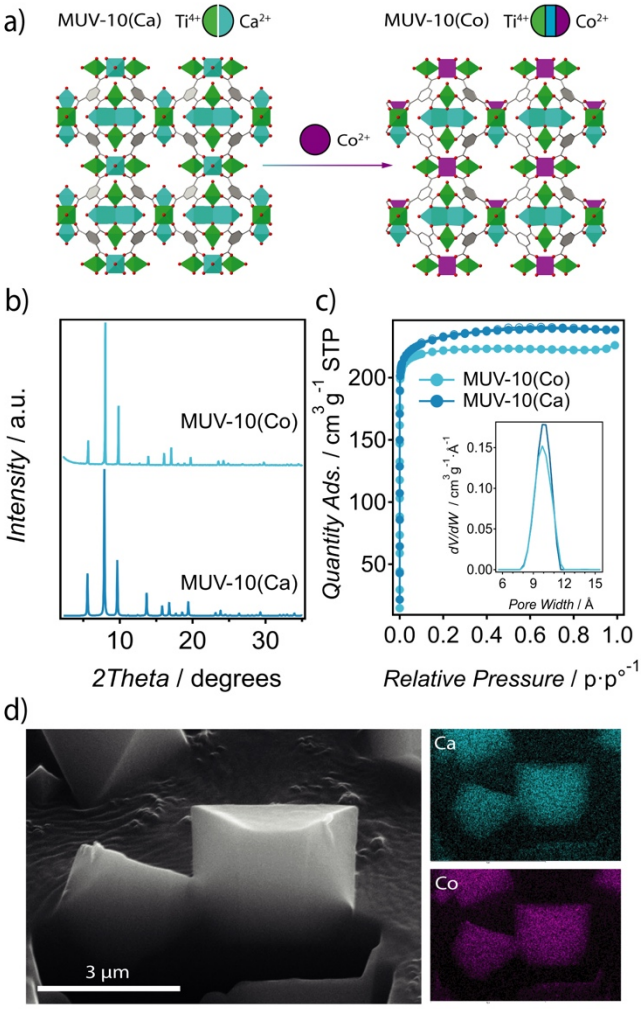

Figure 3. a) Scheme showing the formation of MUV-10(Co) via metal exchange without cluster transformation. b) PXRD of the starting and final materials confirming structural retention, and c) minimum changes in the adsorption isotherm and PSD plot after metal exchange. d) FIB-SEM showing the homogeneous distribution of Ca and Co in the isolated crystals.

submicrometric resolution. As shown in **Figure 3d**, this isostructural exchange occurred homogeneously in all the regions of the crystal. It should be noted that although with the right conditions the effect of metal exchange can be controlled, we have not been able to achieve a complete replacement suggesting that the lower polarity of acetone compared to methanol is effective in blocking the transformation of the cluster but also disfavors the solvation of metal ions.

Framework generalization of Ti_2Ca_2 metal exchange reactivity.

Compared to other post-synthetic transformations reliant on the modification or replacement of the organic linker, this metal-exchange method is controlled by cluster chemistry and thus might be extended to alternative frameworks, provided they are based on the same SBU. To test this hypothesis, we reacted crystals of MUV-12, a single catenated isoreticular **the** net built from 5-tris(4-carboxyphenyl)benzene (H_3btb) linkers with Co^{2+} solutions (**Figure 4a**).[45] The conditions optimized

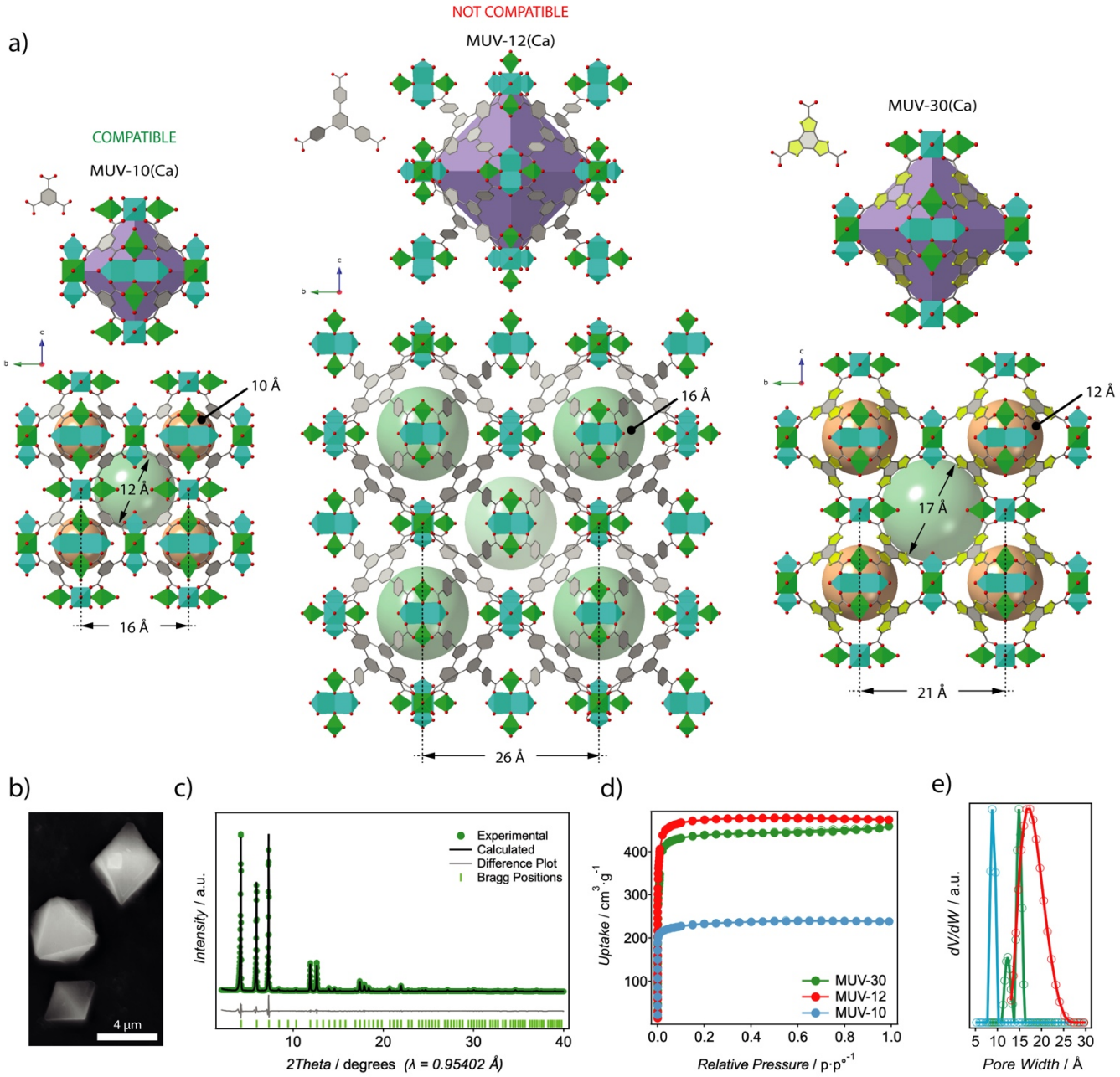

Figure 4. a) Structures of the isoreticular families MUV-10, MUV-12, and MUV-30 formed by connecting 8-connected (8-c) Ti_2Ca_2 clusters with 3-c linkers of variable length (BTC, BTB, and BTB) for the corresponding expansions of the **the** net. Cuboctahedral and octahedral cavities of variable sizes are represented by green and orange spheres, respectively. b) SEM image of octahedral crystal morphology of MUV-30. c) Rietveld refinement confirms the formation of a cubic *Pm-3* structure with a= 20.00970(9) Å (Rwp = 3.82%). d) Type-I N_2 adsorption isotherms at 77 K showing changes in uptake resulting from isoreticular expansion. e) PSD plot confirming the bimodal porosity of MUV-30 and the formation of a cavity very close in size to that in the catenated structure of MUV-12.

with MUV-10 to promote cluster transformation were unsuccessful. Additionally, the use of acetone as a solvent, specifically adapted to promote metal exchange, resulted in cobalt incorporation percentages lower than 10%. (**Supplementary Section S7**). These results suggest that, compared to non-catenated MUV-10, interpenetration forbids cluster transformation and hinders local metal exchange, possibly because of the higher structural rigidity of the framework, which is stabilized by π–π interactions between catenated networks. Based on these results, we thought to extend this reactivity to other non-catenated frameworks that might exhibit similar behavior. We recently described the MUV-12(1,6-naph), (1,4-naph), and (anth) frameworks, for which the use of polyaromatic linkers with high steric hindrance resulted in the formation of partially interpenetrated and non-interpenetrated frameworks with cuboctahedral cavities between 2 and 3 nm in size.[46] Unfortunately, these mesoporous MOFs might impose significant differences based on more favorable mass transfer compared to the micropores in MUV-10 and MUV-12, preventing a meaningful comparison between catenated and non-catenated frameworks with comparable porosity metrics.

To overcome this problem, we designed a new MOF that fulfilled both requirements. We analyzed the tricarboxylic connectors more frequently used in the literature, in which extensions of the central aromatic ring could lead to the assembly of non-interpenetrated frameworks with cavities restricted to microporosity. Based on our work with the MUV-12(X) and (Y) series,[46] we generated, and optimized computationally several Ti_2Ca_2 **the** nets to analyze their thermodynamic preference for the formation of catenated or non-catenated frameworks (**Supplementary Section S.9.1**). Our results identified benzo-tris-thiophene carboxylate acid (H_3BTT) as an adequate choice to prevent translational entanglement and facilitate the assembly of a non-interpenetrated framework with cavities of sizes close to MUV-10 and MUV-12. MUV-30 was synthesized in 5 mL PTFE bottles by reaction of titanium (IV) isopropoxide (35 μmol) with a mixture of calcium chloride (32.5 μmol), acetic acid (800 μL), and H_3BTT (55 μmol) in 3 mL of *N,N*-dimethylformamide (DMF) at 115 °C for 48 h. These conditions were very similar to those previously reported for the growth of MUV-10, MUV-12(X), and MUV-12(Y) crystals.

The solid was isolated as octahedral crystal approximately of 5 μm in size (**Figure 4b**), and the formation of the bimetallic Ti_2Ca_2 cluster was preliminarily confirmed by SEM-EDX and ICP-MS (**Supplementary Section S.8**). Our attempts to solve the structure using synchrotron single-crystal experiments were unsuccessful because of the small size of the crystals. All datasets confirmed the formation of a cubic $Pm\overline{3}$ framework with a cell axis near 21 Å, but they lacked sufficient angular resolution to generate statistically consistent structural models. The structure was solved by Rietveld refinement of the powder diffraction data (**Figure 4c**). As shown in **Figure 4a**, MUV-30 is isoreticular to MUV-10 and confirms the suitability of BTT for directing the assembly of a non-catenated structure with microporous cuboctahedral (coc) and octahedral (oc) cavities of 17 and 12 Å, respectively. The largest one is approximately 40% larger than its equivalent in MUV-10, but very similar to the single cavity present in the interpenetrated structure of MUV-12. This structural analysis agrees well with the N_2 adsorption isotherms and the pore distributions calculated from them (**Figures 4c** and **4d**), which confirmed the microporosity of MUV-30 with a BET surface area of 1750 $cm^3 \cdot g^{-1}$ and a bimodal PSD plot with well-defined peaks centered at 12 (oc) and 15 Å (coc).

We argued that MUV-30 might overcome the limitations of cluster transformation imposed by framework catenation in MUV-12 while imposing a similar mass transfer regime. To confirm this, we incubated fresh crystals of MUV-30 for 24 days in a methanolic solution of Co^{2+} (0.5 M), taking an aliquot after 12 days, which we will refer to as the intermediate stage. The changes observed in the PXRD pattern of the framework suggest a structural transformation characterized by diffraction lines at lower angular values, indicative of cell expansion (**Figure 5a**). Although this was already visible after 12 days, there were residual peaks from the starting MUV-30 phase, indicating an incomplete transformation. These changes agree well with the Ti_2Ca_2 → $TiCo_2$ cluster transformation described above for MUV-10, characterised by a gradual replacement of Ca^{2+} with Co^{2+} until complete conversion for a 2:1 [Co:Ti stoichiometry], according to the ICP analysis of the digested crystals (**Figure 5b**). The framework transformation is related to the overall size and morphology of the crystals used as templating seeds. Like MUV-10, the transformation proceeds by nucleation of a new phase on the surface of the original particles upon metal replacement without imposing dissolution and recrystallisation of the bulk. This agrees well with the segregation of domains rich in Ca and Co that correspond to the original and newly formed phases, which can be resolved by analyzing the cross-section of a partially transformed crystal with FIB-SEM (**Figure 5c**). This segregation disappeared after complete transformation for a homogeneous distribution of metals across the crystal. LeBail refinement of the crystal structure of MUV-301, framework derived from MUV-30, confirms the formation of a cubic $Fd\overline{3}m$ with cell axis of 99.2 Å (**Supplementary Section S.8.3.**).

As shown in **Figure 5d**, the structure of MUV-301 corresponds to an augmented **mtn** net isoreticular to homometallic MIL-100(M_3)[47] and heterometallic MUV-101(TiM_2)[15,36] frameworks. In this case, the formation of augmented supertetrahedra as a result of the expansion of the organic connector leads to the formation of mesoporous cavities of 38 Å (cage 1) and 29 Å (cage 2), built from the interlinking of 24 and 20 supertetrahedra that share their vertices. These values represent an expansion of approximately 30 and 50%, respectively, for the same mesoporous cavities in the framework assembled with BTC. The intermediate and completely transformed MUV-301 crystals were then exchanged with acetone and evacuated at 100 °C under vacuum for 12 h. The N_2 adsorption isotherms showed clear differences compared to those of the starting MUV-30 crystals (**Figure 5f**). The transformation after 12 days triggers an increase in pore volume from 0.72 to 0.96 $cm^3 \cdot g^{-1}$, which agrees well with the incipient formation of the **mtn** topology as corroborated by the sharp jumps in uptake at $p/p_0 = 0.2$ and 0.3. These are more clearly visible after complete transformation, for a total pore volume of 1.62 $cm^3 \cdot g^{-1}$ in MUV-301 (**Supplementary Section S.8.3**). The experimental PSD plots confirmed the evolution of the microporous structure of MUV-30 into the mesoporosity of MUV-301, characterized by the presence of two mesoporous cages centered at 29 and 38 Å, in excellent agreement with the crystallographic structure (**Figure 5g**). If we are not mistaken, MUV-301 is one of the titanium (IV) MOF with the largest pore volume and mesoporous cages reported, only matched by other mesoporous **mtn** materials such as PCN-332/333[48] and Ti^{III}-MIL-101-bpdc.[49] However, these are MOFs based on trivalent metals that can be synthesized by direct synthesis or electrochemical methods. Our experiments indicated that MUV-301 could not be prepared using direct methods (**Supplementary Section S.8.4.**). Unlike MUV-101, which can be isolated from molecular precursors, metal exchange using MUV-30 as a template crystal appears to be the only viable option. The use of BTT does not allow control of the assembly and interlinking with the TiM_2 clusters, which seems to be facilitated by using the Ti_2Ca_2 MOF as a template. In addition, as exemplified before with MUV-10, this structural transformation can be replaced by a strict compositional change by simply adapting the synthetic conditions. The incubation of MUV-30(Ca) crystals in acetone at lower concentrations of Co^{2+} (0.2 M) facilitated the replacement of calcium with shorter reaction times for the formation of MUV-30(Co) (**Figure 5h)**.

Compared to MUV-10, the total replacement of calcium can Compared to MUV-10, the total replacement of calcium can be achieved after three days, as confirmed by ICP analysis (**Figure 5i**). We also used FIB-SEM to map the distribution of both elements in the crystals. As shown in **Figure 5j**, the replacement was complete and perfectly homogeneous throughout the crystal, probably because of the presence of larger pores that facilitated the diffusion of incoming and outcoming cations.

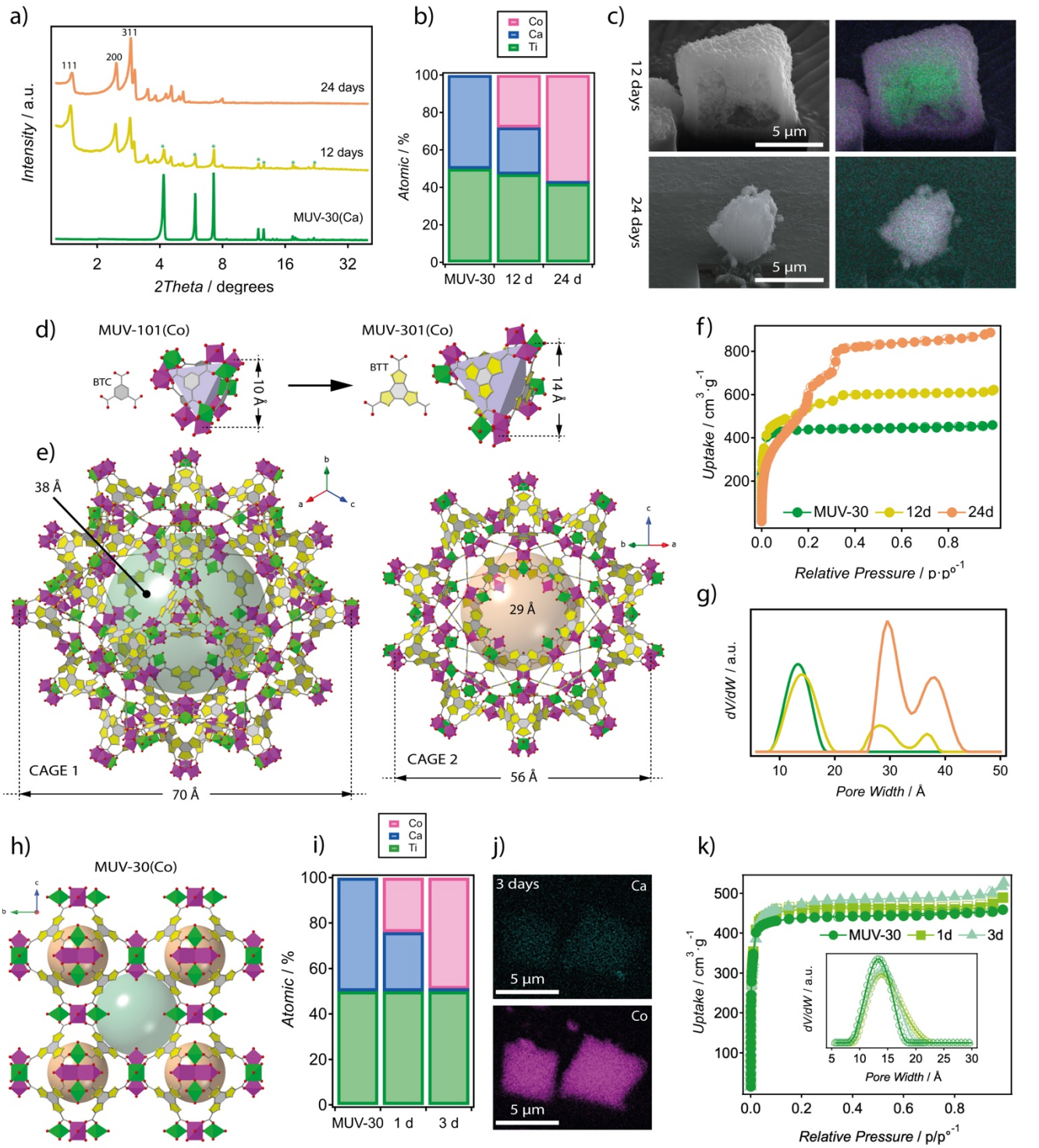

Figure 5. a) Comparison of the PXRD patterns of the starting MUV-30(Ca) with the materials formed after 12 and 24 days of metal exchange. The asterisks highlight the residual diffraction lines of the MUV-30 phase after 12 days, which disappeared completely at the end of the transformation. b) Progression of the relative percentages of metals in the sample obtained by ICP-MS, supporting the formation of a $TiCo_2$ cluster after 24 d. c) FIB-SEM images of the samples after 12 d (top) and 24 d (bottom), confirming the disappearance of the segregation of metals, Ti (green), Ca (blue) and Co (pink), in the crystal at the completion of the transformation. d) Expansion of the supertetrahedra in MUV-101 and MUV-301 because of linker elongation. e) Structures of type 1 and 2 cages in MUV-301 with mesopores near 4 and 3 nm, respectively. f) N_2 isotherms confirming the evolution from microporous to macroporous structure with a larger pore volume as a result of the transformation. g) The PSD plots confirm the evolution of pore sizes until the formation of two mesopores, consistent with those expected for the two cages in MUV-301. h) Proposed structure for MUV-30(Co) prepared by reacting the parent material in acetone to inhibit the cluster transformation. i) Evolution of relative metal ratios with time. j) FIB-SEM was used to confirm the total replacement of original Ca by Co throughout the crystal. k) The N_2 isotherms and corresponding PSD plots rule out any impact on the porosity of the original material.

This behavior is very different from that shown in **Figure 4d**, in which the presence of Ca in the MUV-10 crystals was very clear even after 15 days of exchange. Metal exchange had a negligible impact on the structure and porosity of MUV-30(Co), which displayed a pore volume and PSD plot almost identical to that of the parent calcium MOF (**Figure 5k**).

Effect of chemical diversification on framework electronic properties and photoredox activity.

One of the main possibilities offered by reticular design is to correlate the modification of linkers, cluster composition, and/or structure with the physicochemical properties of the resulting framework. In the context of titanium MOFs, the main interest lies in the effect of this diversification on the photoredox properties of the solid. Previous results with the UCFMOF-n family have shown that the incorporation of varying combinations of linkers constrained to a given topology is an effective tool for tuning electronic properties and mass transfer, both relevant to the control of photocatalytic performance.[50] Studies on MUV-10[41] and MUV-101[51] also revealed that the incorporation of metals, such as Mn^{2+} or Co^{2+}, can be useful for improving the photocatalytic activity of these materials.

To simplify the analysis, we chose to restrict the comparison to the MUV-10 and MUV-30 frameworks because the high number of atoms per unit cell in MUV-101 and 301 was not computationally feasible with the available resources and would require an alternative approach.[52] Furthermore, considering the restrictions imposed by MUV-10 on metal exchange, we consider that the best option to evaluate the effect of Co^{2+} introduction would be to analyze the electronic structures of both MOFs with 50% replacement. The electronic structures and density of states (DOS) diagrams of the four MOFs were calculated using density functional theory (DFT) from either experimental (Ti_2Ca_2) or computationally optimized structures for the mixed-metal systems (Ti_2CaCo). For further details, see **the Supplementary Section S.9.2**. As shown in **Figure 6a** and **b**, replacing BTC with BTT narrows the bandgap of MUV- 30 to 3.1 eV, a value close to that of TiO_2. In contrast, the 4.4 eV calculated for MUV-10 fits well with the theoretical value described in the literature,[53] but is far from the absorption of visible light. This effect is directly controlled by the presence of sulphur in BTT, which contributes to both the highest occupied crystalline orbital (HOCO) and the lowest unoccupied crystalline orbital (LUCO). BTT isomers are often used as hole-transporting materials in solar cells because of their good light absorption, electron-donor character, and ability to generate π-extended systems with good charge mobility.[54] Cobalt incorporation is also positive. MUV-10(Co) and MUV-30(Co) show a bandgap reduction compared to their Ti_2Ca_2 counterparts because of *d*-orbital injection into the HOCO, but this effect is weaker than that achieved by linker replacement.

The optical band gaps obtained from the experimental diffuse reflectance spectra agree well with those calculated for all cases (**Supplementary Section S.10**). Furthermore, the results obtained for MUV-101 and MUV-301(Co) seem to confirm that, in this topology, the presence of BTT also favors visible light absorption over the BTC-based isoreticular analogues for the smallest optical bandgaps of the series, 3.3 and 2.6 eV.

We performed hydrogen photoevolution experiments by irradiating suspensions of the MUV-10, 30, 101, and 301 families in a mixture of methanol and water (30:70 v:v%) with a Xe lamp (300 W). For further experimental details, please refer to the **Supplementary Section S.12.** Although the photodeposition of Pt as a co-catalyst is a common practice to improve the efficiency of this reaction,[55,56] we preferred to avoid it to capture intrinsic ability of these MOFs to photoreduce water. Beyond optimizing the reaction, our goal was to demonstrate the impact of chemical diversification on the properties of the frameworks accessible via metal exchange methods. **Figure 6c** shows the activity of all materials grouped for the same linker into BTC and BTT families. The first striking finding was the negative effect of incorporating Co^{2+}, regardless of linker type and topology. Despite having the largest surface area of the series, MUV-101 and 301, both based on the $TiCo_2$ trimer, showed the lowest activities for nearly 1.000 $\mu mol \cdot g^{-1}$ of H_2 generated after 24 h. This detrimental effect also carries over to the mixed-metal systems, MUV-10(Co) and MUV-30(Co), for which 50% cobalt incorporation results in a loss of activity of 20% and 80%, respectively, compared to their analogues based on the Ti_2Ca_2 cluster. The two systems, MUV-10(Ca) and MUV-30(Ca), showed the best results, with 2.580 and 3.580 μmol of H_2 generated per gram of catalyst, respectively. The improvement in the electronic properties of the MOF anticipated for the presence of BTT can be observed only in this case, although we cannot rule out that the superior porosity of MUV-30 could play an auxiliary role in this enhancement. Although this may be a coincidence, the observed activity ratio was very close to the ratio of the pore volumes of the MUV-10 and MUV-30 nets.

These results suggest that the efficiency of the photoreduction process may not solely depend on light absorption and level alignment, but that the presence of cobalt might also influence the linker-to-metal charge transfer (LMCT) needed to generate catalytically active Ti^{3+} centers. To confirm this possibility, we collected the Electronic Paramagnetic Resonance (EPR) spectra of the MOF series dispersed in acetonitrile. The solvent was purged to remove oxygen and the dispersions were sealed in a quartz tube to prevent Ti^{+3} reoxidation under ambient conditions. Spectra were taken from the same tube at 77 K before and after 12 h of irradiation with ultraviolet light (Kessil PR160L-370 nm). For clarity, **Figure 6d** shows only the region of the spectrum in which the Ti^{3+} resonance (S=1/2) appears with a *g*-factor slightly less than 2.0. Both MUV-10(Ca) and MUV-30(Ca), show an EPR signal at g = 1.93 and 1.91 after irradiation characteristic of Ti(III) photogeneration. These appear together with another line, $g = 2.0$, which is associated with the formation of the organic radical of the linker. MUV-10(Co) and MUV-30(Co) showed no resonances indicative of Ti^{3+} photogeneration and only a very weak resonance at $g = 2.0$, which is insensitive to irradiation and too broad to be an organic radical and is most likely a contribution from high-spin Co^{2+} (S=5/2). In contrast, in MUV-101 and 301, based on the $TiCo_2$ trimers, the linker seems to be responsible for their different behaviors. While MUV-301 only shows resonances associated with the presence of Co^{2+}, MUV-101 does show photogeneration of Ti^{3+} centers with a resonance at $g = 1.94$. Overall, Co^{2+} incorporation inhibits the photogeneration of catalytic centers for Ti_2M_2 clusters regardless of the linker employed, which would explain the lower activity of MUV-10(Co) and MUV-30 (Co) compared to their Ca-based analogues. In contrast, charge transfer in $TiCo_2$-based systems seems to be more influenced by the presence of BTC or BTT linkers. Although the poor activity of MUV-301(Co) is probably due to inefficient LMCT, the performance of MUV-101(Co) does not seem to respond to this reason and must be controlled by other variables.

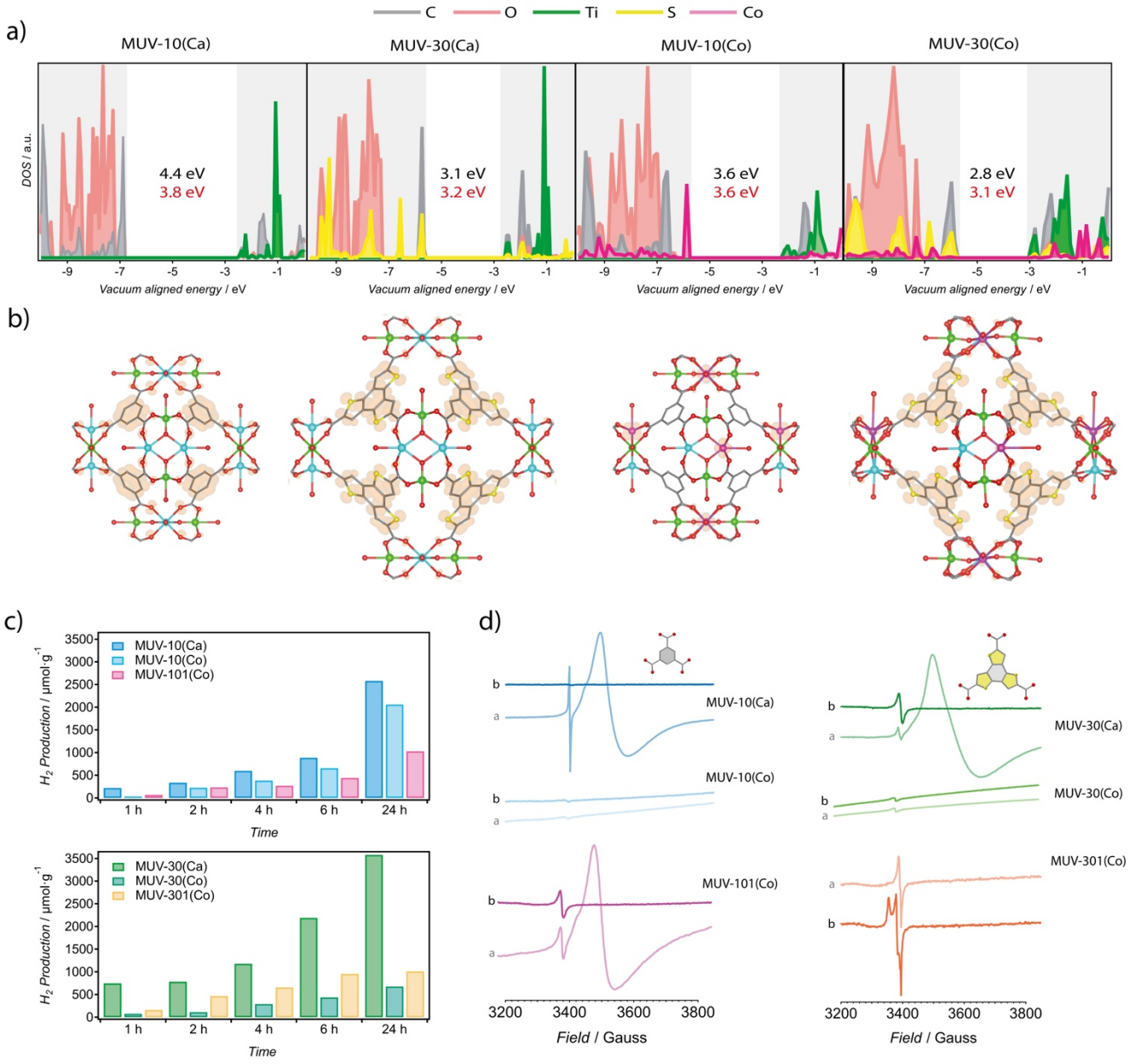

Figure 6. a) Electronic DOS spectra aligned relative to the vacuum level and b) electron density of the highest occupied crystalline orbital of MUV-10(Ca), MUV-30(Ca), MUV-10(Co) and MUV-30(Co). The grey background areas in each plot are the HOCO and LUCO, and the white area between them indicates the theoretical band gap (in black) compared to the experimental value (red) obtained from the Tauc plots. c) Cumulative H_2 photogeneration plots over time grouped by organic connector used in each family: BTC (*top*) and BTT (*bottom*). The activities of MUV-10 and 30 based on the Ti_2Ca_2 cluster present activity maxima for each family. d) EPR spectra of all solids before (dark line) and after (light line) irradiation with a Kessil PR160L-370 nm. Ti^{3+} formation corresponding to resonances with *g*-factors lower than 2.0 is observed only for MUV-10(Ca), MUV-30(Ca), and MUV-101(Co).

CONCLUSION

Perhaps one of the main virtues of reticular design is the richness of the design of porous architectures with diverse structures and compositions. In this study, we introduced the Ti_2Ca_2 cluster metal exchange reaction as a new synthetic tool to conjugate compositional and structural changes, as exemplified for frameworks built from tricarboxylic linkers (BTC, BTB, and BTT). The combination of soft (Ca^{2+}) and hard (Ti^{4+}) coordination bonds in the same SBU can induce two types of metal-exchange reactions. A more conventional "metal substitution" reaction, without significant changes in the structure of the material favored using low-polarity solvents, and a second reaction of transformation of the cluster in polar solvents for the formation of heterometallic titanium-oxo TiM_2 trimers with the consequent transformation of the MOF structure. Once systematized for MUV-10, this methodology was generalized for other isoreticular catenated (MUV-12) and non-catenated (MUV-30) derivatives, demonstrating the impact of interpenetration and pore size on both types of reactivity. The synthesis of MUV-

301, which features mesoporous cages of up to 4 nm in size and the largest pore volume described to date for Ti(IV)-MOFs, also demonstrates the compatibility of metal exchange methods with the design of extended **moo** (or zeolitic **mtn**) topologies that are not accessible by direct synthesis. Finally, we studied the effects of diversifying composition and structure on the electronic structure and photocatalytic activity of this family of titanium MOFs.

We are confident that this methodology will open the door to a greater diversity of titanium frameworks for two primary purposes. From a reticular perspective, the possibility of making this same cluster transformation compatible with other nets derived from 8-c Ti_2Ca_2 nodes could help widen the range of available porous architectures to reach larger 3D mesoporous cages that meet the largest sizes reported to date.[57–59] From a functional point of view, the integration in the same cluster of Ti^{4+} centers with other transition metals will be useful to access specific combinations of metals to control the electronic properties[53,60–62] or catalytic activity[15,51,63–65] of the resulting frameworks.

ASSOCIATED CONTENT

Supporting Information

The Supporting Information is available free of charge on the ACS Publications website.

Synthetic and experimental details; physical characterization and supporting tables and figures (PDF). Crystallographic files by single crystal and Rietveld refinement (CIF).

AUTHOR INFORMATION

Corresponding Author

Natalia M. Padial − Functional Inorganic Materials Team, Instituto de Ciencia Molecular (ICMol), Universitat de València, 46980 València, Spain; orcid.org/0000-00016067-3360; Email: natalia.munoz@uv.es

Carlos Martí-Gastaldo − Functional Inorganic Materials Team, Instituto de Ciencia Molecular (ICMol), Universitat de València, 46980 València, Spain; orcid.org/00000003-3203-0047; Email: carlos.marti@uv.es

Author Contributions

All the authors approved the final version of the manuscript.

Notes

The authors declare no competing financial interests.

ACKNOWLEDGMENT

This work was supported by the H2020 program (ERC-2021-COG-101043428), Generalitat Valenciana (PROMETEU/2021/054, MFA/2022/026, and SEJIGENT/2021/059), and Spanish government (CEX2019-000919-M, CNS2022-135677, PID2020-118117RB-I00). C.C.-G. thanks the Spanish government for the FPI grant (PRE2021-098634). J.C.-G. thanks Generalitat Valenciana for the APOSTD fellowship (CIAPOS/2021/272). N.M.P. thanks the La Caixa Foundation for a Postdoctoral Junior Leader–Retaining Fellowship (ID 100010434, fellowship code LCF/BQ/PR20/11770014). We also thank the University of Valencia for their research facilities (NANBIOSIS) and the Synchotron ALBA for the access to synchrotron radiation at beamlines XALOC (proposal 2022086946) and MSPD (2021035124).

REFERENCES

(1) Freund, R.; Canossa, S.; Cohen, S. M.; Yan, W.; Deng, H.; Guillerm, V.; Eddaoudi, M.; Madden, D. G.; Fairen-Jimenez, D.; Lyu, H.; Macreadie, L. K.; Ji, Z.; Zhang, Y.; Wang, B.; Haase, F.; Wöll, C.; Zaremba, O.; Andreo, J.; Wuttke, S.; Diercks, C. S. 25 Years of Reticular Chemistry. *Angew. Chem. Int. Ed.* **2021**, *60* (45), 23946–23974.

(2) Cadiau, A.; Belmabkhout, Y.; Adil, K.; Bhatt, P. M.; Pillai, R. S.; Shkurenko, A.; Martineau-Corcos, C.; Maurin, G.; Eddaoudi, M. Hydrolytically Stable Fluorinated Metal-Organic Frameworks for Energy-Efficient Dehydration. *Science* **2017**, *356* (6339), 731–735.

(3) Li, L.; Lin, R.-B.; Krishna, R.; Li, H.; Xiang, S.; Wu, H.; Li, J.; Zhou, W.; Chen, B. Ethane/Ethylene Separation in a Metal-Organic Framework with Iron-Peroxo Sites. *Science* **2018**, *362* (6413), 443–446.

(4) Kim, E. J.; Siegelman, R. L.; Jiang, H. Z. H.; Forse, A. C.; Lee, J.-H.; Martell, J. D.; Milner, P. J.; Falkowski, J. M.; Neaton, J. B.; Reimer, J. A.; Weston, S. C.; Long, J. R. Cooperative Carbon Capture and Steam Regeneration with Tetraamine-Appended Metal–Organic Frameworks. *Science* **2020**, *369* (6502), 392–396.

(5) Krause, S.; Bon, V.; Senkovska, I.; Stoeck, U.; Wallacher, D.; Többens, D. M.; Zander, S.; Pillai, R. S.; Maurin, G.; Coudert, F.-X.; Kaskel, S. A Pressure-Amplifying Framework Material with Negative Gas Adsorption Transitions. *Nature* **2016**, *532* (7599), 348–352.

(6) Kim, H.; Yang, S.; Rao, S. R.; Narayanan, S.; Kapustin, E. A.; Furukawa, H.; Umans, A. S.; Yaghi, O. M.; Wang, E. N. Water Harvesting from Air with Metal-Organic Frameworks Powered by Natural Sunlight. *Science* **2017**, *356* (6336), 430–434.

(7) Chen, Z.; Li, P.; Anderson, R.; Wang, X.; Zhang, X.; Robison, L.; Redfern, L. R.; Moribe, S.; Islamoglu, T.; Gómez-Gualdrón, D. A.; Yildirim, T.; Stoddart, J. F.; Farha, O. K. Balancing Volumetric and Gravimetric Uptake in Highly Porous Materials for Clean Energy. *Science* **2020**, *368* (6488), 297–303.

(8) Zhao, M.; Yuan, K.; Wang, Y.; Li, G.; Guo, J.; Gu, L.; Hu, W.; Zhao, H.; Tang, Z. Metal–Organic Frameworks as Selectivity Regulators for Hydrogenation Reactions. *Nature* **2016**, *539* (7627), 76–80.

(9) Jiang, Z.; Xu, X.; Ma, Y.; Cho, H. S.; Ding, D.; Wang, C.; Wu, J.; Oleynikov, P.; Jia, M.; Cheng, J.; Zhou, Y.; Terasaki, O.; Peng, T.; Zan, L.; Deng, H. Filling Metal–Organic Framework Mesopores with TiO2 for CO2 Photoreduction. *Nature* **2020**, *586* (7830), 549–554.

(10) O'Keeffe, M.; Yaghi, O. M. Deconstructing the Crystal Structures of Metal–Organic Frameworks and Related Materials into Their Underlying Nets. *Chem. Rev.* **2012**, *112* (2), 675 702.

(11) Guillerm, V.; Eddaoudi, M. The Importance of Highly Connected Building Units in Reticular Chemistry: Thoughtful Design of Metal–Organic Frameworks. *Acc. Chem. Res.* **2021**, *54* (17), 3298–3312.

(12) Vermoortele, F.; Vandichel, M.; Van de Voorde, B.; Ameloot, R.; Waroquier, M.; Van Speybroeck, V.; De Vos, D. E. Electronic Effects of Linker Substitution on Lewis Acid Catalysis with Metal–Organic Frameworks. *Angew. Chem. Int. Ed.* **2012**, *51* (20), 4887–4890.

(13) Liu, Q.; Cong, H.; Deng, H. Deciphering the Spatial Arrangement of Metals and Correlation to Reactivity in Multivariate Metal–Organic Frameworks. *J. Am. Chem. Soc.* **2016**, *138* (42), 13822–13825.

(14) Ji, P.; Drake, T.; Murakami, A.; Oliveres, P.; Skone, J. H.; Lin, W. Tuning Lewis Acidity of Metal-Organic Frameworks via Perfluorination of Bridging Ligands: Spectroscopic, Theoretical, and Catalytic Studies. *J. Am. Chem. Soc.* **2018**, *140* (33), 10553 10561.

(15) Castells-Gil, J.; Padial, N. M.; Almora-Barrios, N.; Gil-San-Millán, R.; Romero-Ángel, M.; Torres, V.; Silva, I. da; Vieira, B. C. J.; Waerenborgh, J. C.; Jagiello, J.; Navarro, J. A. R.; Tatay, S.; Martí-Gastaldo, C. Heterometallic Titanium-Organic Frameworks as Dual-Metal Catalysts for Synergistic Non-Buffered Hydrolysis of Nerve Agent Simulants. *Chem* **2020**, *6* (11), 3118–3131.

(16) Jia, J.; Gutiérrez-Arzaluz, L.; Shekhah, O.; Alsadun, N.; Czaban-Jóźwiak, J.; Zhou, S.; Bakr, O. M.; Mohammed, O. F.; Eddaoudi, M. Access to Highly Efficient Energy Transfer in Metal–Organic Frameworks via Mixed Linkers Approach. *J. Am. Chem. Soc.* **2020**, *142* (19), 8580–8584.

(17) Hendon, C. H.; Tiana, D.; Fontecave, M.; Sanchez, C.; D'arras, L.; Sassoye, C.; Rozes, L.; Mellot-Draznieks, C.; Walsh, A.

Engineering the Optical Response of the Titanium-MIL-125 Metal-Organic Framework through Ligand Functionalization. *J. Am. Chem. Soc.* **2013**, *135* (30), 10942 10945.

(18) Dou, J.-H.; Arguilla, M. Q.; Luo, Y.; Li, J.; Zhang, W.; Sun, L.; Mancuso, J. L.; Yang, L.; Chen, T.; Parent, L. R.; Skorupskii, G.; Libretto, N. J.; Sun, C.; Yang, M. C.; Dip, P. V.; Brignole, E. J.; Miller, J. T.; Kong, J.; Hendon, C. H.; Sun, J.; Dincă, M. Atomically Precise Single-Crystal Structures of Electrically Conducting 2D Metal–Organic Frameworks. *Nat. Mater.* **2020**, 1–7.

(19) Chen, T.; Dou, J.-H.; Yang, L.; Sun, C.; Libretto, N. J.; Skorupskii, G.; Miller, J. T.; Dincă, M. Continuous Electrical Conductivity Variation in M 3 (Hexaiminotriphenylene) 2 (M = Co, Ni, Cu) MOF Alloys. *J. Am. Chem .Soc.* **2020**, *142* (28), 12367–12373.

(20) Tan, C.; Han, X.; Li, Z.; Liu, Y.; Cui, Y. Controlled Exchange of Achiral Linkers with Chiral Linkers in Zr-Based UiO-68 Metal–Organic Framework. *J. Am. Chem. Soc.* **2018**, *140* (47), 16229–16236.

(21) Chen, X.; Jiang, H.; Hou, B.; Gong, W.; Liu, Y.; Cui, Y. Boosting Chemical Stability, Catalytic Activity, and Enantioselectivity of Metal–Organic Frameworks for Batch and Flow Reactions. *J. Am. Chem. Soc.* **2017**, *139* (38), 13476-13482.

(22) Lv, X.-L.; Yuan, S.; Xie, L.-H.; Darke, H. F.; Chen, Y.; He, T.; Dong, C.; Wang, B.; Zhang, Y.-Z.; Li, J.-R.; Zhou, H.-C. Ligand Rigidification for Enhancing the Stability of Metal–Organic Frameworks. *J. Am. Chem. Soc.* **2019**, *141* (26), 10283–10293.

(23) Jiang, H.; Moosavi, S. M.; Czaban-Jóźwiak, J.; Torre, B.; Shkurenko, A.; Ameur, Z. O.; Jia, J.; Alsadun, N.; Shekhah, O.; Fabrizio, E. D.; Smit, B.; Eddaoudi, M. Reticular Chemistry for the Rational Design of Mechanically Robust Mesoporous Merged-Net Metal-Organic Frameworks. *Matter* **2022**.

(24) Jasuja, H.; Huang, Y.; Walton, K. S. Adjusting the Stability of Metal–Organic Frameworks under Humid Conditions by Ligand Functionalization. *Langmuir* **2012**, *28* (49), 16874 16880.

(25) Lian, X.; Feng, D.; Chen, Y.-P.; Liu, T.; Wang, X.; Zhou, H.-C. The Preparation of an Ultrastable Mesoporous Cr(III)-MOF via Reductive Labilization. *Chem. Sci.* **2015**, *6* (12), 7044 7048.

(26) Senkovska, I.; Bon, V.; Abylgazina, L.; Mendt, M.; Berger, J.; Kieslich, G.; Petkov, P.; Fiorio, J. L.; Joswig, J.-O.; Heine, T.; Schaper, L.; Bachetzky, C.; Schmid, R.; Fischer, R. A.; Pöppl, A.; Brunner, E.; Kaskel, S. Understanding MOF Flexibility: An Analysis Focused on Pillared Layer MOFs as a Model System. *Angew. Chem. Int. Ed.* **2023**, e202218076.

(27) Schneemann, A.; Vervoorts, P.; Hante, I.; Tu, M.; Wannapaiboon, S.; Sternemann, C.; Paulus, M.; Wieland, D. C. F.; Henke, S.; Fischer, R. A. Different Breathing Mechanisms in Flexible Pillared-Layered Metal–Organic Frameworks: Impact of the Metal Center. *Chem. Mater.* **2018**, *30* (5), 1667–1676.

(28) Kalaj, M.; Cohen, S. M. Postsynthetic Modification: An Enabling Technology for the Advancement of Metal–Organic Frameworks. *ACS Cent. Sci.* **2020**, *6* (7), 1046–1057.

(29) Wang, Z.; Cohen, S. M. Postsynthetic Covalent Modification of a Neutral Metal−Organic Framework. *J. Am. Chem. Soc.* **2007**, *129* (41), 12368–12369.

(30) Cohen, S. M. Postsynthetic Methods for the Functionalization of Metal–Organic Frameworks. *Chem. Rev.* **2011**, *112* (2), 970–1000.

(31) Kondo, M.; Furukawa, S.; Hirai, K.; Kitagawa, S. Coordinatively Immobilized Monolayers on Porous Coordination Polymer Crystals. *Angew. Chem. Int. Ed.* **2010**, *49* (31), 5327 5330.

(32) Burnett, B. J.; Barron, P. M.; Hu, C.; Choe, W. Stepwise Synthesis of Metal–Organic Frameworks: Replacement of Structural Organic Linkers. *J. Am. Chem. Soc.* **2011**, *133* (26), 9984–9987.

(33) Karagiaridi, O.; Lalonde, M. B.; Bury, W.; Sarjeant, A. A.; Farha, O. K.; Hupp, J. T. Opening ZIF-8: A Catalytically Active Zeolitic Imidazolate Framework of Sodalite Topology with Unsubstituted Linkers. *J. Am. Chem. Soc.* **2012**, *134* (45), 18790–18796.

(34) Das, S.; Kim, H.; Kim, K. Metathesis in Single Crystal: Complete and Reversible Exchange of Metal Ions Constituting the Frameworks of Metal−Organic Frameworks. *J. Am. Chem. Soc.* **2009**, *131* (11), 3814–3815.

(35) Brozek, C. K.; Dincă, M. Ti3+-, V2+/3+-, Cr2+/3+-, Mn 2+-, and Fe2+-Substituted MOF-5 and Redox Reactivity in Cr- and Fe-MOF-5. *J. Am. Chem. Soc.* **2013**, *135* (34), 12886-12891.

(36) Padial, N. M.; Lerma-Berlanga, B.; Almora-Barrios, N.; Castells-Gil, J.; Silva, I. da; Mata, M. de la; Molina, S. I.; Hernández-Saz, J.; Platero-Prats, A. E.; Tatay, S.; Martí-Gastaldo, C. Heterometallic Titanium–Organic Frameworks by Metal-Induced Dynamic Topological Transformations. *J. Am. Chem. Soc.* **2020**, *142* (14), 6638–6648.

(37) Denysenko, D.; Werner, T.; Grzywa, M.; Puls, A.; Hagen, V.; Eickerling, G.; Jelic, J.; Reuter, K.; Volkmer, D. Reversible Gas-Phase Redox Processes Catalyzed by Co-Exchanged MFU-4 l (Arge). *Chem. Commun.* **2011**, *48* (9), 1236–1238.

(38) Fei, H.; Cahill, J. F.; Prather, K. A.; Cohen, S. M. Tandem Postsynthetic Metal Ion and Ligand Exchange in Zeolitic Imidazolate Frameworks. *Inorg. Chem.* **2013**, *52* (7), 4011–4016.

(39) Song, X.; Jeong, S.; Kim, D.; Lah, M. S. Transmetalations in Two Metal–Organic Frameworks with Different Framework Flexibilities: Kinetics and Core–Shell Heterostructure. *Cryst. Eng. Comm.* **2012**, *14* (18), 5753–5756.

(40) Wei, Z.; Lu, W.; Jiang, H.-L.; Zhou, H.-C. A Route to Metal–Organic Frameworks through Framework Templating. *Inorg. Chem.* **2013**, *52* (3), 1164-1166.

(41) Castells-Gil, J.; Padial, N. M.; Almora-Barrios, N.; Albero, J.; Ruiz-Salvador, A. R.; González-Platas, J.; García, H.; Martí-Gastaldo, C. Chemical Engineering of Photoactivity in Heterometallic Titanium–Organic Frameworks by Metal Doping. *Angew. Chem. Int. Ed.* **2018**, *57* (28), 8453–8457.

(42) Brozek, C. K.; Dinča, M. Cation Exchange at the Secondary Building Units of Metal–Organic Frameworks. *Chem. Soc. Rev.* **2014**, *43* (16), 5456-5467.

(43) Fernández-Conde, C.; Zheng, Y.; Mon, M.; Ribera, A.; Leyva-Pérez, A.; Martí-Gastaldo, C. Time-Resolved Control of Nanoparticle Integration in Titanium-Organic Frameworks for Enhanced Catalytic Performance. *Chem. Sci.* **2024**, *15* (7), 2351–2358.

(44) Prasad, T. K.; Hong, D. H.; Suh, M. P. High Gas Sorption and Metal-Ion Exchange of Microporous Metal–Organic Frameworks with Incorporated Imide Groups. *Chem. Eur. J* **2010**, *16* (47), 14043-14050.

(45) López-Maya, E.; Padial, N. M.; Castells-Gil, J.; Ganivet, C. R.; Rubio-Gaspar, A.; Cirujano, F. G.; Almora-Barrios, N.; Tatay, S.; Navalón, S.; Martí-Gastaldo, C. Selective Implantation of Diamines for Cooperative Catalysis in Isoreticular Heterometallic Titanium–Organic Frameworks. *Angew. Chem. Int. Ed.* **2021**, *60* (21), 11868–11873.

(46) Padial, N. M.; Chinchilla-Garzón, C.; Almora-Barrios, N.; Castells-Gil, J.; González-Platas, J.; Tatay, S.; Martí-Gastaldo, C. Isoreticular Expansion and Linker-Enabled Control of Interpenetration in Titanium–Organic Frameworks. *J. Am. Chem. Soc.* **2023**, *145* (39), 21397–21407.

(47) Ferey, G.; Serre, C.; Mellot-Draznieks, C.; Millange, F.; Surblé, S.; Dutour, J.; Margiolaki, I. A Hybrid Solid with Giant Pores Prepared by a Combination of Targeted Chemistry, Simulation, and Powder Diffraction. *Angew. Chem. Int. Ed.* **2004**, *43* (46), 6296 6301.

(48) Feng, D.; Liu, T.-F.; Su, J.; Bosch, M.; Wei, Z.; Wan, W.; Yuan, D.; Chen, Y.-P.; Wang, X.; Wang, K.; Lian, X.; Gu, Z.-Y.; Park, J.; Zou, X.; Zhou, H.-C. Stable Metal-Organic Frameworks Containing Single-Molecule Traps for Enzyme Encapsulation. *Nat. Commun.* **2015**, *6*, 5979.

(49) Antonio, A. M.; Rosenthal, J.; Bloch, E. D. Electrochemically Mediated Syntheses of Titanium(III)-Based Metal–Organic Frameworks. *J. Am. Chem. Soc.* **2019**, *141* (29), 11383–11387.

(50) Bryant, J. T.; Logan, M. W.; Chen, Z.; Djokic, M.; Cairnie, D. R.; Vazquez-Molina, D. A.; Nijamudheen, A.; Langlois, K. R.; Markley, M. J.; Pombar, G.; Holland, A. A.; Caranto, J. D.; Harper, J. K.; Morris, A. J.; Mendoza-Cortes, J. L.; Jurca, T.; Chapman, K. W.; Uribe-Romo, F. J. Synergistic Steric and Electronic Effects on the Photoredox Catalysis by a Multivariate Library of Titania Metal–Organic Frameworks. *J. Am. Chem. Soc.* **2023**, *145* (8), 4589–4600.

(51) Wang, Y.; Lv, H.; Grape, E. S.; Gaggioli, C. A.; Tayal, A.; Dharanipragada, A.; Willhammar, T.; Inge, A. K.; Zou, X.; Liu, B.; Huang, Z. A Tunable Multivariate Metal–Organic Framework as a Platform for Designing Photocatalysts. *J. Am. Chem. Soc.* **2021**, *143* (17), 6333–6338.

(52) Protesescu, L.; Calbo, J.; Williams, K.; Tisdale, W.; Walsh, A.; Dincă, M. Colloidal Nano-MOFs Nucleate and Stabilize Ultra-Small

Quantum Dots of Lead Bromide Perovskites. *Chem. Sci.* **2021**, *12* (17), 6129–6135.

(53) Fabrizio, K.; Lazarou, K. A.; Payne, L. I.; Twight, L. P.; Golledge, S.; Hendon, C. H.; Brozek, C. K. Tunable Band Gaps in MUV-10(M): A Family of Photoredox-Active MOFs with Earth-Abundant Open Metal Sites. *J. Am. Chem. Soc.* **2021**, *143* (32), 12609–12621.

(54) Molina-Ontoria, A.; Zimmermann, I.; Garcia-Benito, I.; Gratia, P.; Roldán-Carmona, C.; Aghazada, S.; Graetzel, M.; Nazeeruddin, M. K.; Martín, N. Benzotrithiophene-Based Hole-Transporting Materials for 18.2 % Perovskite Solar Cells. *Angew. Chem. Int. Ed.* **2016**, *55* (21), 6270–6274.

(55) Sun, K.; Qian, Y.; Jiang, H. Metal-Organic Frameworks for Photocatalytic Water Splitting and CO2 Reduction. *Angew. Chem. Int. Ed.* **2023**, *62* (15), e202217565.

(56) Navalón, S.; Dhakshinamoorthy, A.; Álvaro, M.; Ferrer, B.; García, H. Metal–Organic Frameworks as Photocatalysts for Solar-Driven Overall Water Splitting. *Chem. Rev.* **2023**, *123* (1), 445–490.

(57) Liu, Q.; Song, Y.; Ma, Y.; Zhou, Y.; Cong, H.; Wang, C.; Wu, J.; Hu, G.; O'Keeffe, M.; Deng, H. Mesoporous Cages in Chemically Robust MOFs Created by a Large Number of Vertices with Reduced Connectivity. *J. Am. Chem. Soc.* **2018**, *141* (1), 488–496.

(58) Hu, G.; Liu, Q.; Zhou, Y.; Yan, W.; Sun, Y.; Peng, S.; Zhao, C.; Zhou, X.; Deng, H. Extremely Large 3D Cages in Metal–Organic Frameworks for Nucleic Acid Extraction. *J. Am. Chem. Soc.* **2023**.

(59) Barsukova, M.; Sapianik, A.; Guillerm, V.; Shkurenko, A.; Shaikh, A. C.; Parvatkar, P.; Bhatt, P. M.; Bonneau, M.; Alhaji, A.; Shekhah, O.; Balestra, S. R. G.; Semino, R.; Maurin, G.; Eddaoudi, M. Face-Directed Assembly of Tailored Isoreticular MOFs Using Centring Structure-Directing Agents. *Nat. Synth.* **2023**, 1–14.

(60) Syzgantseva, M. A.; Ireland, C. P.; Ebrahim, F. M.; Smit, B.; Syzgantseva, O. A. Metal Substitution as the Method of Modifying Electronic Structure of Metal-Organic Frameworks. *J. Am. Chem. Soc.* **2019**, *141* (15), 6271–6278.

(61) Rice, A. M.; Leith, G. A.; Ejegbavwo, O. A.; Dolgopolova, E. A.; Shustova, N. B. Heterometallic Metal–Organic Frameworks (MOFs): The Advent of Improving the Energy Landscape. *ACS Energy Lett.* **2019**, *4* (8), 1938–1946.

(62) Ejegbavwo, O. A.; Berseneva, A. A.; Martin, C. R.; Leith, G. A.; Pandey, S.; Brandt, A. J.; Park, K. C.; Mathur, A.; Farzandh, S.; Klepov, V. V.; Heiser, B. J.; Chandrashekhar, M.; Karakalos, S. G.; Smith, M. D.; Phillpot, S. R.; Garashchuk, S.; Chen, D. A.; Shustova, N. B. Heterometallic Multinuclear Nodes Directing MOF Electronic Behavior. *Chem. Sci.* **2020**, *11* (28), 7379–7389.

(63) Buchwalter, P.; Rosé, J.; Braunstein, P. Multimetallic Catalysis Based on Heterometallic Complexes and Clusters. *Chem. Rev.* **2015**, *115* (1), 28–126.

(64) Abednatanzi, S.; Derakhshandeh, P. G.; Depauw, H.; Coudert, F.-X.; Vrielinck, H.; Voort, P. V. D.; Leus, K. Mixed-Metal Metal–Organic Frameworks. *Chem. Soc. Rev.* **2019**, *48* (9), 2535–2565.

(65) Rubio-Gaspar, A.; Navalón, S.; Tatay, S.; Cirujano, F. G.; Fernández-Conde, C.; Padial, N. M.; Martí-Gastaldo, C. Metal Node Control of Brønsted Acidity in Heterobimetallic Titanium–Organic Frameworks. *J. Am. Chem. Soc.* **2023**, *145* (7), 3855–3860.